Higher order spherical harmonics reconstruction of fetal diffusion MRI with intensity correction

Maria Deprez[a,*], Anthony Price[a], Daan Christensen[a], Georgia Lockwood Estrin[b], Lucilio Cordero-Grande[a], Alessandro Daducci[e], Donald Tournier[a], Mary Rutherford[b], Serena Counsell[b], Merixtell Bach Cuadra[c,d], Joseph V. Hajnal[a]

[a] *Deparment of Biomedical Engineeeing, King's College London*
[b] *Department of Perinatal Imaging, King's College London*
[c] *EPFL, Signal Processing Laboratory 5 (LTS5)*
[d] *Radiology Department, Lausanne University Hospital; Center for Biomedical Imaging (CIBM), Lausanne University*
[e] *University of Verona, Computer Science, Verona, Italy*

Abstract

We present a comprehensive method for reconstruction of fetal dMRI signal using a higher order spherical harmonics representation. We show that intensity correction improves the consistency of the volumetric reconstruction. By applying constrained spherical deconvolution and whole brain tractography to reconstructed fetal dMRI we are able to identify main WM tracts and anatomically plausible fiber crossings. The proposed methodology facilitates detailed investigated of developing brain connectivity and microstructure in-utero.

Keywords: fetal diffusion MRI, spherical harmonics, motion correction, distortion correction, intensity correction, tractography

1. Introduction

Fetal diffusion MRI (dMRI) can provide detailed insights into healthy development of brain connectivity and microstructure in pre-natal period. The fetal diffusion imaging is however very challenging due the fetal motion, maternal breathing, geometric distortion of echo planar imaging (EPI), spin history

*Corresponding author
Email address: maria.murgasova@kcl.ac.uk (Maria Deprez)

artefacts due to long relaxation times of water-rich fetal brain tissues, and significant intensity inhomogeneity and low resolution resulting from tiny fetal head being embedded inside the mother's body. Early studies therefore relied on sequences that required very short acquisition time [1] or selecting the datasets least affected by motion [2].

Motion correction and scattered data interpolation. Duration of acquisition of one EPI slice is typically around 300 ms and most of the slices are therefore not significanly affected by motion. However, motion is almost always present between individual slices. Jiang *et al.* [3] therefore proposed to use slice-to-volume registration (SVR) to correct for between-slice motion, similarly to previously proposed aproach for motion correction of structural fetal MRI [4, 5]. Unlike in structural MRI, different dMRI slices correspond to different sensitation gradients which change with respect to fetal brain anatomy according to the motion parameters. Jiang *et al.* [3] therefore proposed to register the diffusion data to the reconstructed (non-sensitised) B0 volume using normalised mutual information as a similarity measure, followed by model-based approach, where each slice is registered to the simulated volume with corresponding sensitation gradient. Another challenge - reconstruction of diffusion tensor on isotropic grid from data scattered in both spatial and angular domain, has been addressed by using an interpolation model and inverting a large sparse matrix to calculate a consistent isotropic volume of diffusion tensors. Oubel *et al.* [6] has shown, that co-registration of slices of arbitraty gradient sensitations using cross-correlation as a similarity measure is more robust than registrering them to B0 image using normalised mutual information and this approach is also successfully adopted in this paper. To perform scattered data interpolation, they perform radial basis function (Gaussian) interpolation in both spatial and angular domains. Model-based approach that combines interpolation using Gaussian process in angular domain with volumetric registration has been shown to allow for motion correction of adult data with very high b-values (up to $b = 7000$) [7], however, fetal data are subject to much larger motion and b-values are limited to up to

approximatelly $b = 1000$ due to limited signal to noise ratio.

Super-resolution reconstruction. Due to the insufficient signal-to-noise ratio and coverage of the brain, fetal dMRI has been traditionally acquired using thick-slice sequences, with slice thickness typically set to twice the in-plane resolution. Due to this fact, super-resolution aprroach has been proposed for fetal structural MRI [8, 9, 10] and later also for fetal dMRI [11]. Though thick-slice approaches are still most common for acquisition fetal dMRI in clinical settings, novel isotropic fetal dMRI sequences, which will be a topic of another publication, have been developed as a part of developing Human Connectomme Project (dHCP). However, even in this context, the concept of modelling of acquisition of the slice using a point-spread-function (PSF) based on principles of MR physics [10] remains valid, avoidning the smoothing properties of interpolation methods, though the resulting method does not comprise "super-resolution" any more. In this paper we therefore adapt such inverse problem approach, generalising the estimation of regular isotropic dMRI volume from scattered data to isotropic and unisotropic acquisitions.

Geometric distortion. Major issue when reconstructed fetal dMRI is geometric distortion of EPI acquisition. We have addressed this problem by registration of acquired B0 images to reconstructed structural data that are not subject the distortion with physically inspired Laplacian constraint [12] and this approach is applied and validated in this paper. Further improvement - dynamic time-varying distortion correction - is being developed as a part of dHCP and will be a topic of another publication.

Spin history effects. Relaxation times (T1 and T2) of fetal brain tissues are significanly higher than for adult brain due to high water content of fetal brain tissues. To avoid spin history effects, time between slice-selective excitation of the same location (repetition time TR) has to be sufficiently long. This becomes impractical, as a lot of scanning time is lost waiting for recovery of the magnetisation, limiting the number of diffusion direction that can be acquired. The

problem is further complicated in presence of motion, where sufficient TR cannot be garanteed because of uncertainty of anatomical location of each excited slice. Therefore a compromise has to be made between spin history artefacts and image quality and spin history correction has to be incorporated into the reconstruction of the diffusion volume. We have addressed this problem by data-driven approach for structural MRI [10], where low frequency slice-wise bias fields were estimated to match intensities of slices to the reconstructed volume. We have also sucessfully implemented similar approach for dMRI in this paper. Alternative strategy is to model spin history effects based on estimated motion parameters and principles of MR physics, as we previously proposed for fetal functional MRI (fMRI)[13] and this remains an area of future research for fetal dMRI. When motion disrupts the acquisition to the point that slice is corrupted we employ robust statistics proposed by us [10] and adapted for dMRI to exclude the corrupted slices.

Bias field. Acquisition is further corrupted by B1 inhomogeneity, stemming from inhomogeneity of receive and transmit B1 field. We employ the method previously proposed for fetal fMRI [13] and correct the B1 effects in the preprocessing step by estimating B1 field fromn B0 images and applying them to diffusion sensitised images. Alternative method has been developed by Seshamani *et al.* [14] and could be used instead if sufficient number of B0 stacks in different motion states are present.

Spatial and angular regularisation. In case of super-resolution reconstruction fetal structural MRI, the reconstructed isotropic volume needs to be regularised to prevent noise enhancement due to the inverse problem being ill-posed. Various regularisation terms have been proposed, including L2 norm [8], edge-preserving regularisation [9, 10] and L1 norm [15]. Most common regulariser in angular domain is Laplace-Bertrami operator [16]. In our current experiments we have not identified a significant benefit of the regularisation for our test data and this will be investigated in future.

Beyond diffusion tensor. Previous methods for reconstruction of fetal dMRI were limited to diffusion tensor, mainly due to the data quality not supporting higher order models. Diffusion tensor however does not allow for modelling of crossing fibers and is therefore too restrictive for the state-of-the-art fetal dMRI acquisition sequences, such as the ones being developed for dHCP. In adult studies, one of the most popular way to parametrise dMRI in angular domain is using Spherical Harmonics (SH) [17, 16], though non-parametric models such as Gaussian Process [7, 18] have been used as well. Previously, it has been shown, that by using SH model, fiber crossings can be identified in fetal dMRI [19]. However, this work relies on assumption of no fetal motion in the data.

Contribution of this paper. In this paper we propose a novel framework to perform reconstruction of fetal dMRI signal from scattered data using spherical harmonics (SH) parametrisation of the diffusion signal, which allows for modelling of crossing fibers. We show that given sufficient angular resolution and b-value, we are able identify anatomically plausible fiber crossings by performing constrained spherical harmonics deconvolution [17] of the reconstructed dMRI signal. We also show that intensity artefacts such as B1 inhomogeneity and motion induced spin history effects need to be corrected to obtain consistent reconstructions.

2. Methods

2.1. Reconstruction of Spherical Harmonics representation of dMRI signal from scattered data

Spherical Harmonics representation. Our aim is to estimate SH representation C of fetal dMRI signal $\bar{s}$ on high-resolution isotropic grid represented by index i

$$\bar{s}_i(\vec{g}) = \sum_{lm} c_{i,lm} Y_{lm}(\vec{g}) \tag{1}$$

where $\vec{g}$ represents diffusion direction, $c_{i,lm}$ stand for SH coefficients and Y_{lm} are real SH basis functions of order m.

The forward model. The acquired signal is denoted s_{jk} , where index k represents a slice and j represents an in-plane grid point of a slice. The simulation $\bar{s}_{jk}$ of an acquired slice s_{jk} can be decomposed into the following steps. First, we simulate high resolution volume $\bar{s}_i(\vec{g_k})$ from SH coefficients C using the diffusion gradient $\vec{g}_k$ associated with the slice k. Point-spread-function m_{ij}^k, which takes into account in-plane resolution, slice thickness, position and orientation of the fetal head in the scanner space at the time of acquisition [10], is then applied to simulate the signal $\bar{s}_{jk}$ for each voxel in the slice:

$$\bar{s}_{jk} = \sum_i m_{ij}^k \bar{s}_i(\vec{g}_k) \tag{2}$$

The objective function. The underlying SH representation C can then be estimated by minimising the objective function

$$F(C) = \frac{1}{2} \sum_{jk} (s_{jk} - \bar{s}_{jk})^2$$

that represents sum of squared differences between acquired and simulated signal. The objective function is optimised iteratively using gradient descent

$$c_{i,lm}^{(n+1)} = c_{i,lm}^{(n)} + \alpha \sum_{jk} (s_{jk} - \bar{s}_{jk}^{(n)}) m_{ij}^k Y_{lm}(\vec{g}_k) \tag{3}$$

where n denotes the iteration number.

2.2. Intensity matching

Spin history effects can be modelled to a good approximation as a slice-wise smoothly varying multiplicative fields $e^{b_{jk}}$. The B1 inhomogeneity can be considered approximatelly stationary in the scanner space and will therefore modulate data in the space of the fetal head differently as the fetus moves. We however do not consider these differential bias field effects separately, but consider them as being included in the $e^{b_{jk}}$. The objective function then becomes

$$F(C, B) = \sum_{jk} (s_{jk} - e^{b_{jk}} \bar{s}_{jk})^2 \tag{4}$$

There are many ways to impose smoothness on the fields b_{jk}, either parametric, by modelling it as a linear combination of the basis functions, or non-parametric by imposing a smoothness penalty. In case of parametric representation the smoothness is imposed by restricting the number of control points (or the basis functions), while in the non-parametric cases the covariance matrix $\Psi_{k,\sigma}$ for b_{jk} can be defined instead. If b_{jk} are drawn form multidimensional Gaussian distribution $N(0, \Psi_{k,\sigma})$, then the bias fields are modelled as a Gaussian processes. This is equivalent to parametric representation using regularised dense linear combination of Gaussian radial basis functions. We prefer the non-parametric model, because it results in more flexible space of solutions. However, it requires inversion of matrix of dimension J_kxJ_k where J_k is a number of pixel in a slice k. Inspired by work of Wells *et al.* [20] and proposed by us [10], we therefore approximate the estimation of the residual bias fields $\Delta b_{jk}^{(n+1)}$ by weighted kernel regression

$$\Delta b_{jk}^{(n+1)} = \frac{\sum_l r_{lk}^{(n+1)} w_{lk}^{(n+1)} G_\sigma(d_{lk})}{\sum_l w_{lk}^{(n+1)} G_\sigma(d_{lk})} \tag{5}$$

applied to residuals

$$r_{jk}^{(n+1)} = \log\left(\frac{s_{jk}}{\bar{s}_{jk} e^{b_{jk}^{(n)}}}\right) \tag{6}$$

where d_{lk} is distance between grid points l and k and G_σ represents Gaussian kernel with standard deviation σ that regulates the smoothness of the bias fields. The weights $w_{lk} = \bar{s}_{jk} e^{b_{jk}^{(n)}}$ ensure that the residual resuting from division by a small number are down-weighted as these are likely to reflect noise, while voxels with high signals drive the estimation. If the voxel-wise robust statistics is used as in [10], the weights can also include posterior probability that the voxel belongs to the inlier class. The bias fields can then be expressed as

$$b_{jk}^{(n+1)} = b_{jk}^{(n)} + \Delta b_{jk}^{(n+1)} \tag{7}$$

2.3. The algorithm

Pre-processing. The algorithm starts by several pre-processing steps, where the dMRI is brain-masked (semi-automatically), bulk B1 bias field is estimated

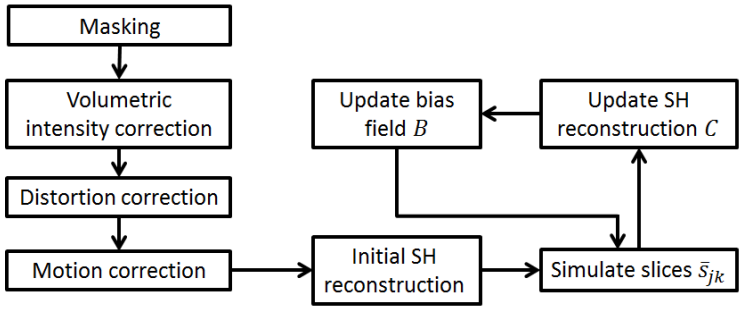

Figure 1: Processing pipeline

using (non-sensitised) b0 volumes [13] and corrected for all diffusion sensitised volumes. The stationary B0 field inhomogeneity induced distortion is estimated by registration of b0 volumes to the T2 weighted ssFSE reconstructed volume of the same subject [12] and applied to the diffusion sensitised volumes. The motion is then estimated using slice-to-volume registration (SVR) [10] applied to all the diffusion sensitised volumes, irrespective of the diffusion directions and with normalised cross-correlation as a similarity measure, as proposed previously [6].

Initialisation. The estimated motion parameters are combined with acquisition specific PSF to calculate acquired voxel specific PSFs m_{ij}^k that take into account position in space and motion parameters. The reconstructed high-resolution volume, that is the output of SVR [10] applied to all diffusion sensitised volumes irrespective of the sensitation gradient can be interpreted as a zero-order ($m = 0$) SH representation of dMRI signal and used for initialisation of SH reconstruction $C^{(0)}$. Bias fields b_{jk} are initialised as zero fields. Slice-specific diffusion gradients $\vec{g}_k$ are calculated by rotating nominal volume-specific gradient vectors from the pre-defined gradient table using rotation component of the slice-specific motion parameters.

The algorithm. The isotropic SH representation C of the fetal dMRI signal is estimated by minimising the objective function F (eqn. 4) using gradient descent (GD). The algorithm proceeds by iterating between three steps:

1. Simulate slices $\bar{s}_{jk}^{(n)}$ from SH representation $C^{(n)}$ using eqn. (1) and (2).
2. Update SH representation $C^{(n+1)}$ using eqn. (3).
3. Update bias fields $B^{(n+1)}$ using eqn. (5), (6) and (7).

If corrupted slices are present, an additional robust statistics step can be included, in a similar manner as described in our previous work for fetal structural MRI [10]. The whole processing pipeline is summarised in Fig. 1.

3. Experiments

3.1. Acquisition of fetal dMRI

1.5T anisotropic dataset. Fetal dMRI of six subjects (gestational ages 24, 26, 29, 32, 33 and 34 weeks) was acquired on a 1.5T Philips Achieva scanner using spin echo EPI sequence with one b0 volume and 15 diffusion sensitised volumes with b=500 s/mm^2, TE 121ms, TR 8500ms, voxel size 2.3x2.3x3.5mm^3, slice overlap 1.75mm. Acquisition time was approximatelly 5 minutes.

3T anisotropic dataset. Diffusion MRI of additional three fetal subjects (gestational ages 32, 33 and 35 weeks) were acquired on a 3T Phillips Achieva scanner using spin echo EPI sequence with three b0 volumes and 32 diffusion sensitised volumes with b=750 s/mm^2, TE 75ms, TR 7500ms, voxel size 2x2x3.5mm^3, slice overlap 1.75mm. Acquisition time was approximatelly 5 minutes.

3T isotropic dataset. A single dMRI fetal dataset (gestational age 25 weeks) that was acquired as a part of developing Human Connectomme Project (dHCP) during sequence development stage was considered in this work. The dataset was acquired on a 3T Phillips Achieva scanner using double spin echo EPI sequence with 140 volumes on three shells (b=0, 400 and 1000 s/mm^2). Only the top shell and the first echo volumes were considered in this paper, resulting in 80 b=1000 s/mm^2 diffusion sensitised volumes, with TE 75ms, TR 7500ms, voxel size 2x2x2mm^3, slice gap 0mm. Acquisition time for the whole dataset was approximatelly 15 minutes. For this particular dataset a phase-based dynamic distortion correction was applied.

3.2. Implementation

Brain masking. Brain-masking was performed using a semi-automatic approach, where all diffusion weighted volumes were registered using volumetric registration, averaged and the average image was then thresholded, followed by sequence of morphological operations to obtain the brain mask.

Intensity matching. The Gaussian kernel that regulates smoothness of the bias field in the pre-processing step as well as during SH reconstruction was experimentally set to $\sigma = 20$mm.

Motion correction. We have performed three motion correction iterations, that iterleaved slice-to-volume registration with recostrution of a single volume. The first iteration was constrained registration of whole stacks of slices, in second iteration stacks were split to even and odd slices in accordance with the acquisition order and in the final iteration slices were registered to the reconstructed volume independently.

Reconstruction of SH representation. During SH reconstruction we performed ten GD iterations, that interleave simulation of the slices, updating the SH representation and bias fields. We have observed that the value of the objective function F (eqn. 4) was decreasing at every iteration, so there was not an obvious threshold for stopping the algorithm. However, visual inspection confirmed, that quality of reconstruction did not significanly increase after 10 iterations and this was also a good compromise in terms of computational time.

SH order. Maximum viable order for SH representation is dictated by number of volumes of different diffusion directions and the b-value. For 1.5T dataset, we have observed that the acquisition protocol and $b = 500$ only supported 2nd order SH model, even though theoretically, 15 directions are the minimum requirement for 4th order model. We therefore performed 2nd order reconstructions, which are equivalent to diffusion tensor and do not support reconstruction of fiber crossings. For 3T datasets we used higher order model (4th order for

3T anisotropic and 6th order for 3T isotropic) which allow for identification of crossing fibers.

Running time. The algorithm was parallelised using TBB (Intel Threaded Building Blocks library). The reconstructions were performed on a desktop PC with 24 threads and lasted approximatelly 15 minutes per subject.

3.3. Quantitative evaluation

We have performed quantitative evaluation of two important elements of the pipeline: distortion correction and intensity matching for 9 fetal subjects (1.5T and 3T anisotropic datasets). We excluded 5 diffusion sensitised volumes for each subject and reconstructed the SH represetnation of the dMRI signal using remaining 10 volumes for 1.5T dataset and 27 volumes for 3T dataset. The slices of the excluded stacks were then simulated from the reconstructed SH representation and compared to the acquired stacks.

To perform qantitative comparison we calculate root mean squared error (RMSE) between simulated and acquired stacks for three different cases: The pipeline without distortion correction and intensity matching (*basic*), with distortion correction by no intensity matching (*dist*) and the full pipeline with both distortion correction and intensity matching (*dist-int*).

3.4. Constrained spherical deconvolution and whole brain tractography

Evaluation of accuracy of slice to volume reconstruction of fetal MRI is difficult due to lack of ground truth. Previous works [5, 3, 8, 10, 6, 11] used simulated experiments, where motion corrupted data are simulated from non-motion-corrupted dataset and RMSE or PSNR between original and reconstructed data is calculated. However, these experiments, though valuable, cannot fully capture the challenges of reconstruction in presence of all acquisition artefacts. Additionally, a global numerical average error can be quite a poor indicator whether the correct structure is present in the reconstructed data. As similar approaches that aim at reconstruction of diffusion tensor have been evaluated using simulated experiments in previous works [6, 11], we opt for an alternative approach,

in which we visualise and assess the structure captured by our reconstructed fetal data. To do that, we perform constrained spherical deconvolution [17] to estimate fiber orientation density function followed by whole brain tractography using MRtrix3 software package [21] available from `www.mrtrix.org`. We will assess the reconstructed data for the presence of the main white matter tracts and the 3T isotropic and anisotropic datasets will be evaluated for the presence of the fiber crossings.

4. Results

4.1. Distortion correction

The effect of distortion correction was evaluated calculation of RMSE between five excluded stacks and their simulation the SH representation as described in Sec. 3.3, that was reconstructed with (*dist*) and without (*basic*) distortion correction step. Results in Table 1 show that distortion correction improves RMSE for each subject, from average value 8.21 to 8.12. Two-tail student t-test confirmed that this result was significant ($p = 2.3 \times 10^{-3}$).

	GA	Dataset	*basic*	*dist*	*dist-int*
Subj 1	24	1.5T	9.89	9.79	**9.40**
Subj 2	26	1.5T	9.72	9.51	**8.59**
Subj 3	29	1.5T	6.19	6.16	**5.49**
Subj 4	32	1.5T	7.45	7.39	**6.91**
Subj 5	33	1.5T	9.88	9.77	**8.54**
Subj 6	34	1.5T	5.78	5.67	**5.51**
Subj 7	32	3T	8.12	7.94	**6.03**
Subj 8	33	3T	8.68	8.66	**7.82**
Subj 9	35	3T	8.20	8.16	**7.09**
average			8.21	8.12	**7.30**

Table 1: RMSE between acquired and simulated stacks that were excluded from the reconstruction for 9 fetal subjects. Pipelines compared: Basic pipeline without distortion and intensity correction (*basic*); Pipeline with distortion correction but without intensity matching (*dist*); Full pipeline with distortion correction and intensity matching (*dist-int*).

4.2. Intensity matching

The effect of intensity matching was evaluated by comparing RMSE (Sec. 3.3) for the pipeline without (*dist*) and with (*dist-int*) the intensity matching. The results in Table 1 show substantial improvement in RMSE, from 8.12 to 7.30 ($p = 1.7 \times 10^{-3}$). The effect of intensity matching on the consistency of the intensities on the acquired data is shown in Fig. 2.

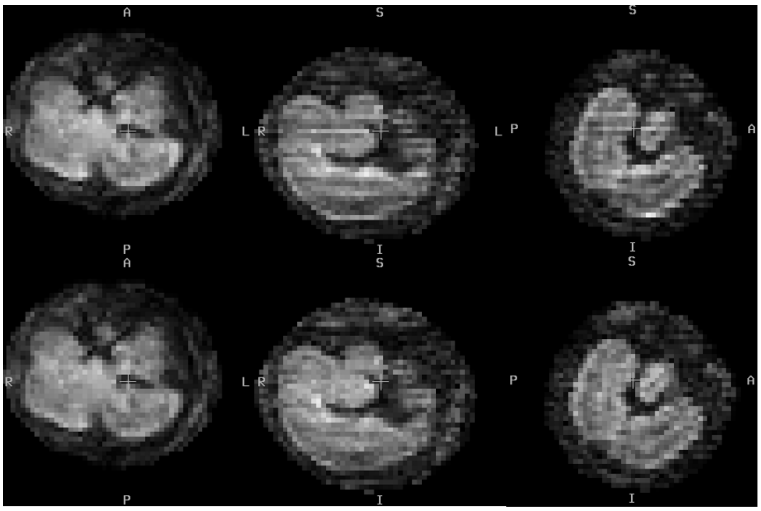

Figure 2: The effect of intensity matching on the acquired data. An original stack is displayed in the top row. The intensity corrected stack after application of estimated bias fields b_{jk} is displayed in the bottom row. Note that the spin history artefact resulting in stripes in the original data in the through-plane direction (second and third view, top row) disappeared in the corrected data (second and third view, bottom row).

4.3. Assesment of reconstructed fetal dMRI

Visual inspection of the whole brain tractography confirmed that main white matter tracts could be identified in all 9 fetal subjects, including corpus callosum, cortico-spinal tract, superior longitudinal fasciculus and cingulum. The whole brain tractography of the three fetal subjects (3T anisotropic dataset) with fiber crossings of these tracts is depicted in Fig. 3.

In Fig. 4 we present the fiber orientation distribution (FOD) functions and whole brain tractography of the fetal subject from the isotropic 3T dataset with

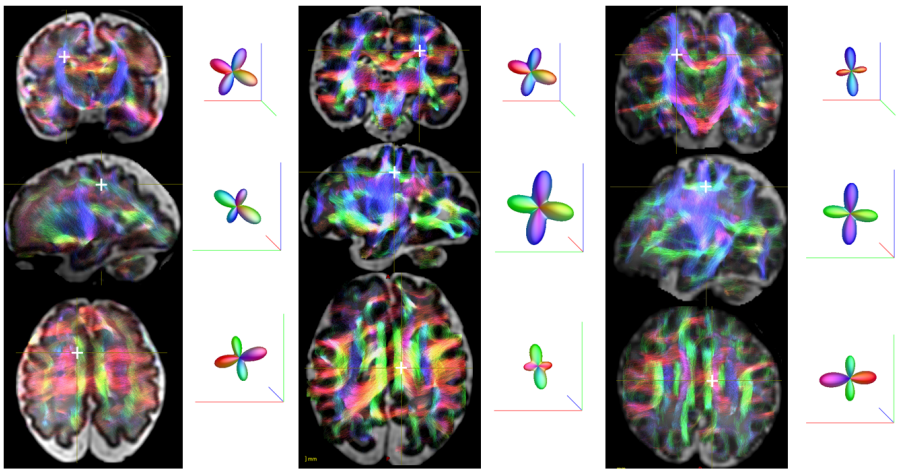

Figure 3: Whole brain tractography of three fetal subjects from 3T anisotropic dataset (32, 33 and 35 weeks GA, first, second and third column respectively) overlayed on the reconstructed T2 weighted (ssFSE) anatomical image. The tractography correctly depicts main white matter tracts, colour coded as follows: Red left-right, e.g. corpus callossum (CC); Blue top-bottom e.g. cortico-spinal tract (CST); Green front-back, e.g. superior longitudinal fasciculus (SLF) and cingulum (CG). The fiber crossings: First row: CC and CST; Second row: CST and SLF; third row: CC and CG.

80 diffusion directions and b=1000. We can clearly obbserve features typical of young fetuses, including radial orientation of the FODs in the smooth cortical ribbon and smooth structure consisting only of the major WM tracts and radially oriented fibers, where differentiation observed in older fetuses (Fig. 3) is not present yet.

5. Conclusion

In this paper we proposed a comprehensive framework for reconstruction of fetal dMRI using higher-order SH representation that corrects for motion, distortion, spin history and bias field artefacts. We have demonstrated that the reconstructed isotropic fetal dMRI signal can be used to perform constrained spherical deconvolution and whole brain tractography commonly used for analysis of dMRI in adult subjects. As a result, a comprehensive investigation of the

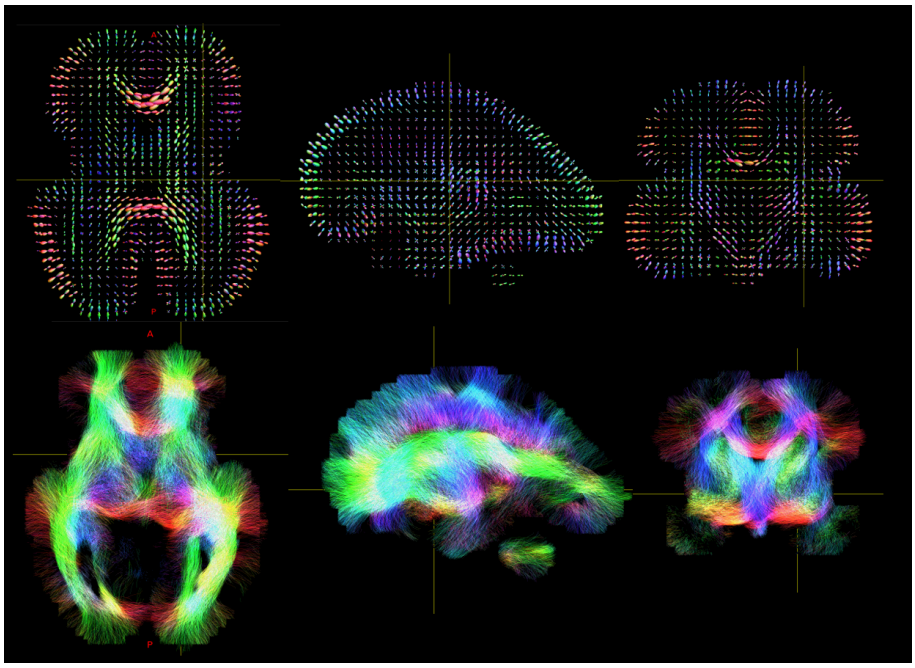

Figure 4: Fiber orientation distribution (FOD) functions (top row) and whole brain tractography (bottom row) of the 3T isotropic fetal dataset (25 weeks GA). In addition to the main WM tracts we can also observe features specific to young fetal subjects, in particular radially oriented FODs within the smooth cortical ribbon (top row) and radially oriented fibers and smooth structure of cortical hemisheres, due to the anatomy typical of more mature subjects not being developed yet.

in-vivo in-utero brain development is possible for the first time, including timing of the development of various WM tracts and presence of the developmental features such as radial orientation within the fetal cortex. The higher order SH model also supports reconstruction of anatomically plausible fiber crossings in the developing fetal brain. The proposed methodology facilitates standard diffusion analysis in fetal population, opening opportunities for in depth investigation of developing fetal brain connectivity and microstructure.

References

[1] D.-H. Kim, S. Chung, D. B. Vigneron, A. J. Barkovich, O. A. Glenn, Diffusion-weighted imaging of the fetal brain in vivo, Magnetic Resonance in Medicine 59 (1) (2008) 216–220.

[2] G. Kasprian, P. C. Brugger, M. Weber, M. Krssak, E. Krampl, C. Herold, D. Prayer, In utero tractography of fetal white matter development, NeuroImage 43 (2) (2008) 213 – 224.

[3] S. Jiang, H. Xue, S. Counsell, M. Anjari, J. Allsop, M. Rutherford, D. Rueckert, J. V. Hajnal, Diffusion tensor imaging (DTI) of the brain in moving subjects: Application to in-utero fetal and ex-utero studies, Magnetic Resonance in Medicine 62 (3) (2009) 645–655.

[4] F. Rousseau, O. A. Glenn, B. Iordanova, C. Rodriguez-Carranza, D. B. Vigneron, J. A. Barkovich, C. Studholme, Registration-based approach for reconstruction of high-resolution in utero fetal MR brain images, Academic Radiology 13 (9) (2006) 1072 – 1081.

[5] S. Jiang, H. Xue, A. Glover, M. Rutherford, D. Rueckert, J. Hajnal, MRI of moving subjects using multislice snapshot images with volume reconstruction (SVR): Application to fetal, neonatal, and adult brain studies, IEEE Transactions on Medical Imaging 26 (7) (2007) 967 –980.

[6] E. Oubel, M. Koob, C. Studholme, J.-L. Dietemann, F. Rousseau, Reconstruction of scattered data in fetal diffusion MRI, Medical Image Analysis 16 (1) (2012) 28 – 37.

[7] J. L. Andersson, S. N. Sotiropoulos, An integrated approach to correction for off-resonance effects and subject movement in diffusion MR imaging, NeuroImage 125 (2016) 1063 – 1078.

[8] A. Gholipour, J. Estroff, S. Warfield, Robust super-resolution volume reconstruction from slice acquisitions: Application to fetal brain MRI, IEEE Transactions on Medical Imaging 29 (10) (2010) 1739 –1758.

[9] F. Rousseau, K. Kim, C. Studholme, M. Koob, J.-L. Dietemann, On super-resolution for fetal brain MRI, in: Medical Image Computing and Computer Assisted Intervention, 2010.

[10] M. Kuklisova-Murgasova, G. Quaghebeur, M. A. Rutherford, J. V. Hajnal, J. A. Schnabel, Reconstruction of fetal brain MRI with intensity matching and complete outlier removal, Medical Image Analysis 16 (8) (2012) 1550 – 1564.

[11] M. Fogtmann, S. Seshamani, C. Kroenke, X. Cheng, T. Chapman, J. Wilm, F. Rousseau, C. Studholme, A unified approach to diffusion direction sensitive slice registration and 3-D DTI reconstruction from moving fetal brain anatomy, Medical Imaging, IEEE Transactions on 33 (2) (2014) 272–289.

[12] M. Kuklisova-Murgasova, G. L. Estrin, R. G. Nunes, S. J. Malik, M. A. Rutherford, D. Rueckert, J. V. Hajnal, Distortion correction in fetal epi using non-rigid registration with a laplacian constraint, IEEE Transactions on Medical Imaging 37 (1) (2018) 12–19.

[13] G. Ferrazzi, M. K. Murgasova, T. Arichi, C. Malamateniou, M. J. Fox, A. Makropoulos, J. Allsop, M. Rutherford, S. Malik, P. Aljabar, J. V. Hajnal, Resting state fMRI in the moving fetus: A robust framework for motion, bias field and spin history correction, NeuroImage 101 (2014) 555 – 568.

[14] S. Seshamani, X. Cheng, M. Fogtmann, M. E. Thomason, C. Studholme, A method for handling intensity inhomogenieties in fmri sequences of moving anatomy of the early developing brain, Medical Image Analysis 18 (2) (2015) 285–300.

[15] S. Tourbier, X. Bresson, P. Hagmann, J.-P. Thiran, R. Meuli, M. B. Cuadra, An efficient total variation algorithm for super-resolution in fetal brain MRI with adaptive regularization, NeuroImage 118 (2015) 584 – 597.

[16] M. Descoteaux, E. Angelino, S. Fitzgibbons, R. Deriche, Regularized, fast, and robust analytical q-ball imaging, Magnetic Resonance in Medicine 58 (3) 497–510.

[17] J.-D. Tournier, F. Calamante, A. Connelly, Robust determination of the fibre orientation distribution in diffusion mri: Non-negativity constrained super-resolved spherical deconvolution, NeuroImage 35 (4) (2007) 1459 – 1472.

[18] J. L. Andersson, M. S. Graham, I. Drobnjak, H. Zhang, N. Filippini, M. Bastiani, Towards a comprehensive framework for movement and distortion correction of diffusion mr images: Within volume movement, NeuroImage 152 (2017) 450 – 466.

[19] J. Pontabry, F. Rousseau, E. Oubel, C. Studholme, M. Koob, J.-L. Dietemann, Probabilistic tractography using q-ball imaging and particle filtering: Application to adult and in-utero fetal brain studies, Medical Image Analysis 17 (3) (2013) 297 – 310.

[20] W. Wells III, W. Grimson, R. Kikinis, F. Jolesz, Adaptive segmentation of MRI data, IEEE Transactions on Medical Imaging 15 (4) (1996) 429–442.

[21] J.-D. Tournier, F. Calamante, A. Connelly, Mrtrix: Diffusion tractography in crossing fiber regions, International Journal of Imaging Systems and Technology 22 (1) (2012) 53–66.